PLANT SCIENCES

WUSCHEL-RELATED HOMEOBOX 13 suppresses de novo shoot regeneration via cell fate control of pluripotent callus

Nao Ogura[1,2], Yohei Sasagawa[3,4], Tasuku Ito[2,5], Toshiaki Tameshige[1,6], Satomi Kawai[2], Masaki Sano[2]†, Yuki Doll[1], Akira Iwase[7], Ayako Kawamura[7], Takamasa Suzuki[8], Itoshi Nikaido[3,4], Keiko Sugimoto[7,9], Momoko Ikeuchi[1,2,7]*

Plants can regenerate their bodies via de novo establishment of shoot apical meristems (SAMs) from pluripotent callus. Only a small fraction of callus cells is eventually specified into SAMs but the molecular mechanisms underlying fate specification remain obscure. The expression of WUSCHEL (WUS) is an early hallmark of SAM fate acquisition. Here, we show that a WUS paralog, WUSCHEL-RELATED HOMEOBOX 13 (WOX13), negatively regulates SAM formation from callus in *Arabidopsis thaliana*. WOX13 promotes non-meristematic cell fate via transcriptional repression of *WUS* and other SAM regulators and activation of cell wall modifiers. Our Quartz-Seq2–based single cell transcriptome revealed that WOX13 plays key roles in determining cellular identity of callus cell population. We propose that reciprocal inhibition between WUS and WOX13 mediates critical cell fate determination in pluripotent cell population, which has a major impact on regeneration efficiency.

INTRODUCTION

Plants are characterized by their outstanding regenerative capacity to reconstruct entire individuals from somatic cells (*1*). A critical step in the reconstruction of entire bodies is a de novo reconstruction of a shoot apical meristem (SAM), composed of stem cells, stem cell niches, and transit-amplifying cells, which perpetually give rise to lateral organs. Extensive molecular genetic studies using tissue culture of *Arabidopsis thaliana* (*Arabidopsis*) have uncovered gene regulatory mechanisms underlying SAM initiation during organ regeneration (*2*). In a widely used two-step tissue culture system, root or hypocotyl explants are firstly incubated on auxin-rich callus-inducing media (CIM) to generate pluripotent calli and subsequently transferred to cytokinin-rich shoot-inducing media (SIM) to induce de novo establishment of SAM (Fig. 1A) (*3*). During incubation on CIM, auxin induces the formation of pluripotent callus via root meristem formation pathway (*4*, *5*). PLETHORA 3 (PLT3), PLT5, and PLT7 play pivotal roles in pluripotency acquisition by up-regulating *PLT1/2* and *CUP-SHAPED COTYLEDON 1* (*CUC1*) and *CUC2* (*5*). PLT1 and PLT2 together with WUSCHEL-RELATED HOMEOBOX 5 (WOX5) directly induce an auxin synthesis enzyme gene *TRYPTOPHAN AMINOTRANSFERASE OF ARABIDOPSIS 1* (*TAA1*) to confer cellular pluripotency (*6*). Upon transfer to SIM, activated cytokinin signaling directly up-regulates *WUSCHEL* (*WUS*), which is a key step in SAM formation (*7*). *WUS* is indispensable for shoot regeneration from callus and an early marker gene of shoot fate acquisition (*7*, *8*). Noteworthy, WUS is activated in a small subset of callus cells (*7*), and only a fraction of WUS-expressing cell clusters eventually become SAMs, which is regulated by the localized expression of an auxin transporter PIN-FORMED 1 (PIN1) together with CUC2 (*9*). CUC1 and CUC2, in turn, promote shoot meristem formation via transcriptional up-regulation of SHOOT MERISTEMLESS (*STM*) (*10*). Apart from hormonal and developmental regulations, wounding signals also play important roles in inducing shoot regeneration. *WOUND-INDUCED DEDIFFERENTIATION 1* (*WIND1*) mediates this process via direct transcriptional induction of *ENHANCER OF SHOOT REGENERATION 1* (*ESR1*) (*11*).

Whereas the above-described regulatory pathways stimulate SAM formation, plants also have negative regulations that restrict shoot regeneration from callus. Several epigenetic regulations maintain repressive status of target gene loci, thereby hindering cellular fate transition from callus to SAM. For instance, *WUS* locus has repressive chromatin status in callus cells that needs to be transcriptionally activated to enable shoot regeneration (*7*). Loss-of-function mutation of *DNA METHYLTRANSFERASE 1* (*MET1*) or *POLYCOMB REPRESSIVE COMPLEX 2* (*PRC2*) leads to enhanced shoot regeneration, suggesting that erasing these repressive marks facilitates de novo SAM establishment (*12*, *7*). Similarly, a repressive histone variant H2A.Z restricts regeneration efficiency, which seems to mediate temperature responses (*13*). A SUMO E3 ligase, *SAP AND MIZ1 DOMAIN-CONTAINING LIGASE1* (SIZ1), negatively regulates de novo shoot formation, potentially through suppressing the stress response (*14*). The interplay between these positive and negative regulations collectively determines the developmental output as shoot regeneration efficiency. However, how

[1]Division of Biological Sciences, Graduate School of Science and Technology, Nara Institute of Science and Technology, 8916-5, Takayama-cho, Ikoma, Nara 630-0192, Japan. [2]Department of Biology, Faculty of Science, Niigata University, Niigata, Niigata 950-2181, Japan. [3]Department of Functional Genome Informatics, Division of Medical Genomics, Medical Research Institute, Tokyo Medical and Dental University, Bunkyo, Tokyo, Japan. [4]RIKEN Center for Biosystems Dynamics Research, Wako, Saitama 351-0198, Japan. [5]Institute of Science and Technology Austria, Am Campus 1, 3400 Klosterneuburg, Austria. [6]Kihara Institute for Biological Research, Yokohama City University, 641-12 Maioka, Yokohama 244-0813, Japan. [7]RIKEN Center for Sustainable Resource Science, Yokohama, Kanagawa 230-0045, Japan. [8]Department of Biological Chemistry, College of Biosciences and Biotechnology, Chubu University, Kasugai, Aichi 487-8501, Japan. [9]Department of Biological Sciences, The University of Tokyo, Bunkyo-ku, Tokyo 119-0033, Japan.
*Corresponding author. Email: momoko.ikeuchi@bs.naist.jp
†Present address: Department of Biology, Division of Advanced Science and Engineering, Graduate School of Science and Engineering, Chiba University, 1-33, Yayoi-cho, Inage-ku, Chiba, Chiba 263-8522, Japan.

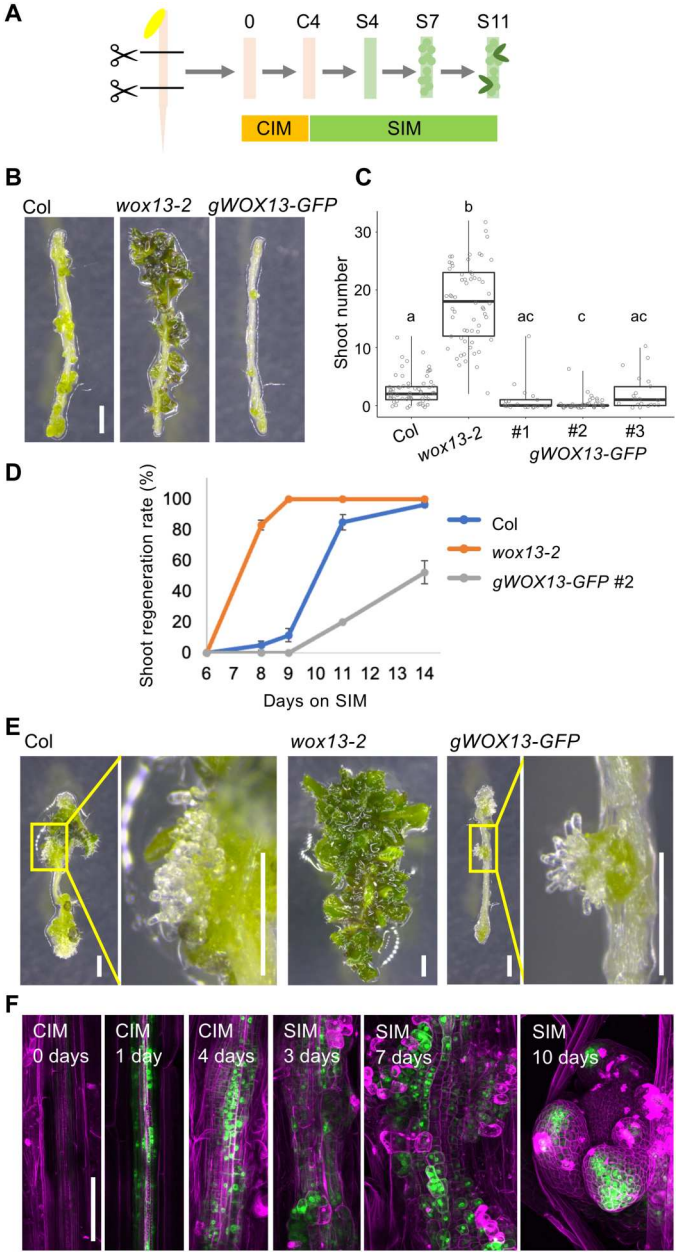

Fig. 1. WOX13 suppresses shoot regeneration from pluripotent callus. (**A**) Schematic diagram of tissue culture procedure. Hypocotyl explants from etiolated seedlings were incubated on CIM for 4 days and then transferred to SIM for further incubation. (**B** and **C**) Shoot regeneration phenotype of *wox13-2* mutant and the complementing line (*gWOX13-GFP* in *wox13-2*). Representative images of explants (B) and quantitative data of shoot number per explant on SIM at day 11 (C). Alphabetical letters indicate statistical significance determined by analysis of variance (ANOVA) and Tukey's multiple comparisons test ($n \geq 40$, $P < 0.05$). (**D**) Time-series examination on shoot regeneration phenotype ($n \geq 2$, 20 explants for each replicate). Shoot regeneration rate shows the frequency of explants that bear at least one shoot. (**E**) Representative images of explants on SIM at day 14. The inset shows the magnified image of the explant of Col and *gWOX13-GFP*, where highly expanded globular cells are present. (**F**) Spatiotemporal expression of *gWOX13-GFP* during tissue culture incubation. WOX13 expression is visualized by GFP (green) and cellular outlines are visualized by propidium iodide (PI) staining (magenta). Scale bars, 1 mm (B) and (E) and 0.1 mm (F).

these regulatory interplay acts at the cellular level to specify cell fate to be or not to be SAM remains elusive.

The advent of single-cell transcriptome technologies is revolutionizing developmental biology and regenerative biology (*15*). The application of single-cell RNA sequencing (scRNA-seq) analysis to plant tissues encountered additional technical hurdles due to the encapsulation of plant cells inside cell walls and the larger cell size. Nevertheless, the application is becoming widespread and facilitates the discovery of novel regulatory genes (*16*–*20*). A recent study exploiting scRNA-seq uncovered specific gene expression profile of the middle layer of the callus formed on CIM, where pivotal genes for pluripotency acquisition are expressed (*6*). On the other hand, a repertory of callus cells during shoot formation on SIM is yet to be characterized at the transcriptome level. In this study, we found that WOX13 suppresses de novo shoot regeneration from callus. By exploiting Quartz-Seq2–based scRNA-seq analyses, we obtained the cell atlas of heterogeneous callus and emerging SAMs. Our scRNA-seq analyses revealed that *wox13* mutant callus displays prominent difference in cellular composition, highlighting the critical role of WOX13 in cell fate specification in callus.

RESULTS

WOX13 suppresses de novo shoot formation from pluripotent callus

We recently identified WOX13 as a pivotal regulator of tissue repair and organ adhesion upon grafting (*21*). To test potential roles of WOX13 in the control of shoot regeneration, we analyzed the *wox13* mutant phenotype in a two-step tissue culture system using hypocotyl explants (*3*). We found that the *wox13* mutant generates significantly higher abundance of shoots after 11 days of incubation on SIM (Fig. 1, B and C). Our time series observation further revealed that shoot regeneration in the *wox13* mutant is accelerated by 3 days compared to wild type (WT; Fig. 1D). The enhanced shoot regeneration phenotype of the *wox13* mutant was complemented by introducing *WOX13* genomic fragment fused with green fluorescent protein (*gWOX13-GFP*), demonstrating that *WOX13* represses de novo shoot formation (Fig. 1, B and C). Furthermore, a transgenic line with strong *gWOX13-GFP* signal displayed significantly lower shoot regeneration efficiency than WT (Fig. 1C and fig. S1). The observed anticorrelation between GFP signal intensity and shoot regeneration efficiency between independent lines further corroborates the repressive role of WOX13 on shoot regeneration. We also found that an additional cytological phenotype that highly expanded callus cells that cover WT explants are mostly missing from the *wox13* mutant explants (Fig. 1E). The formation of highly expanded, globular cells in callus is also rescued in *gWOX13-GFP* lines (Fig. 1E). This cytological phenotype of the *wox13* mutant is reminiscent of callus formed at wound sites (*21*), highlighting the commonality in cytological phenotypes among different callus types. Thus, we conclude that WOX13 restricts the capacity of calli to regenerate shoots while promoting cellular differentiation to highly expanded globular cells.

We next analyzed the spatiotemporal expression pattern of *gWOX13-GFP* using the complementing line. Whereas WOX13 was not expressed in intact etiolated hypocotyls, the expression initiated within 1 day after incubation on CIM (Fig. 1F), which is in line with the previous study showing that WOX13 is

transcriptionally induced upon cutting and auxin treatment (*21*, *22*). Furthermore, comparison between incubation of explants on CIM or hormone-free media revealed that incubation on CIM strongly enhanced WOX13 expression (fig. S2A), implicating that the hormonal cue in CIM, not the cutting stimuli during explant preparation, is responsible for *WOX13* induction. We further dissected the effect of auxin (2,4-D) and cytokinin (kinetin) to conclude that the auxin is primarily responsible for the up-regulation of WOX13 expression on CIM (fig. S2B). *gWOX13-GFP* was broadly expressed in callus cell population during incubation on CIM and SIM (Fig. 1F). After 10 days on SIM, WOX13 was totally absent from the established SAM, whereas the signal is detected in leaf primordia. The depletion of WOX13 expression from the SAM is in accordance with its inhibitory role in SAM formation. Together, our phenotypic and imaging analyses revealed that WOX13 is a negative regulator of shoot regeneration, whose expression is induced upon incubation and is locally reduced in SAMs.

Shoot meristem regulators and cell wall modifiers are misexpressed in the *wox13* mutant

To elucidate how WOX13 affects gene expression profile during callus formation and shoot regeneration, we performed time course comparative RNA-seq between WT and the *wox13* mutant at day 0, CIM at day 4, SIM at day 4, and SIM at day 7 on tissue culture (table S1). Note that any cytological or morphological differences were undetectable between the genotypes on SIM at day 4, whereas calli of each genotype were markedly different on SIM at day 7. Namely, emerging or established SAMs are highly abundant in the *wox13* mutant calli, while SAMs are rarely observed in WT calli on SIM ay day 7.

We performed a pairwise comparison of the genotypes at each time point using edgeR with thresholds of false discovery rates (FDRs) < 0.01 (table S2) (*23*). This analysis revealed that 144 genes were up-regulated and 385 genes were down-regulated in the *wox13* mutant on day 0 (fig. S3). Gene ontology (GO) categories enriched in the differentially expressed genes (DEG) on day 0 include response to various stimuli. These genes likely respond to the drastic environmental changes during explant preparation including the cutting stimuli and the shift from the dark to light. It

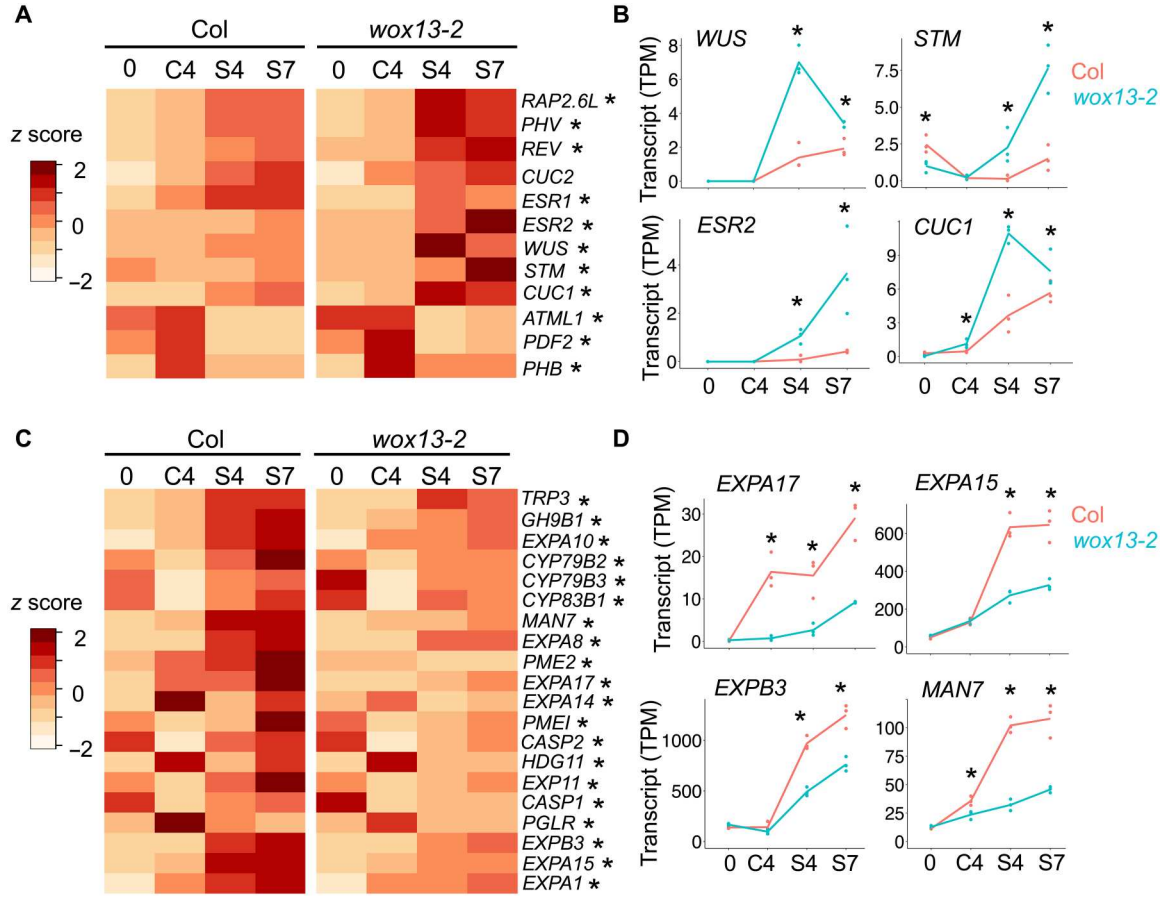

Fig. 2. Shoot meristem regulators and cell wall modifiers are misregulated in the *wox13* mutant. (**A**) Heatmap graphs showing the expression of genes involved in shoot meristem formation. Genes that display significantly different expression in at least one time point are highlighted by asterisks (edgeR, $P < 0.05$). (**B**) Representative examples of DEGs in (A) retrieved from RNA-seq dataset. Asterisks show significant difference at respective time points (edgeR, $P < 0.05$). The expression is shown in Transcripts Per Kilobase Million (TPM). (**C**) Heatmap graphs showing the expression of genes listed in the GO category "cell wall modification." (**D**) Representative examples in (C) retrieved from RNA-seq dataset. Asterisks show significant difference at respective time points (edgeR, $P < 0.05$). Time course expression data were obtained on day 0 (0), CIM at day 4 (C4), SIM at day 4 (S4), and SIM at day 7 (S7).

is plausible that WOX13 is involved in a wide range of stress responses, although whether they are relevant to regenerative responses is currently unknown. The number of DEG markedly dropped on CIM at day 4, where only 11 genes are up-regulated and 31 genes are down-regulated in the mutant (fig. S3). After transfer to SIM, growing number of genes are up-regulated (495 on SIM at day 4 and 996 genes on SIM at day 7) or down-regulated (488 genes on SIM at day 4 and 806 genes on SIM at day 7). The overall transcriptome profiling indicates that the *wox13* mutation does not have prominent impacts on callus formed on CIM, although WOX13 is strongly expressed, and misexpression becomes evident during subsequent incubation on SIM.

Next, we focused on GO categories that are up-regulated in the *wox13* mutant (table S3). Functional categories such as meristem initiation (4.55×10^{-7}) and shoot system morphogenesis (1.43×10^{-5}) are highly represented on SIM at day 4 and SIM at day 7, as expected from the enhanced shoot regeneration phenotype (fig. S3A). We thus compared the expression of selected genes that are functionally characterized to regulate pluripotency acquisition and shoot regeneration during tissue culture (*2*). We compared the expression of key genes in pluripotency acquisition to find out that most of these genes displayed a similar trend of slightly higher expression in *wox13* mutant (fig. S4A). However, the magnitude of difference was rather subtle, and only *PLT5* displayed significantly higher expression in the *wox13* mutant. As expected, our imaging analysis failed to detect any difference in *pWOX5::ER-GFP* (*24*) expression on CIM at day 4 (fig. S4B), further suggesting that the expression of pluripotency genes in callus on CIM at day 4 was not markedly affected. We next analyzed genes that are involved in shoot fate acquisition. We found that the expression level of *WUS*, *CUC1*, *ESR2*, *RAP2.6L*, *PHB*, *PHV*, and *STM* was significantly elevated on SIM at day 4, whereas the expression of *CUC2* and *ESR1* was either unaffected or down-regulated depending on the time points (Fig. 2, A and B). Given that the timing of elevated expression of these shoot regulator genes was earlier than that of any detectable cytological differences, it is most likely that the gene expression change is a direct consequence of *wox13* mutation rather than any indirect outcome accompanying enhanced shoot formation phenotype.

Within down-regulated GO categories (table S3), a functional category "cell wall loosening" (2.68×10^{-7}) is highly enriched during incubation on SIM (fig. S3B). Genes involved in cell wall modification such as *EXPANSIN A1* (*EXPA1*), *EXPA8*, *EXPA10*, *EXP11*, *EXPA14*, *EXPA15*, *EXPA17*, *EXPB3*, *PECTIN METHYL ESTERASE 2* (*PME2*), and *MANNASE 7* (*MAN7*) are markedly down-regulated in the *wox13* mutant (Fig. 2, C and D). Noteworthy, similar genes involved in cell wall modification were previously identified to be wound inducible in a WOX13-dependent manner (*21*), corroborating the idea that WOX13 generally regulates cell wall–related processes. We also noted that auxin homeostasis (9.04×10^{-5}) was highly represented in the GO analysis (fig. S3B); thus, we compared *DR5rev::GFP* expression in callus cells on CIM and SIM to test potential differences in cellular auxin response. *DR5rev::GFP* signal was broadly detected in callus cell population and locally depleted from the growth foci on CIM at day 4 (fig. S5). The expression was strongly detected in inner layers of calli on SIM as reported previously (fig. S5) (*25*). We did not to find any detectable differences in the signal intensity or spatial pattern of *DR5rev::GFP* either on CIM at day 4 or SIM at day 4 (fig. S5); thus, we conclude that cellular auxin responses are not actually affected in the *wox13* mutant.

WOX13 suppresses the expression of shoot meristem regulators and induces cell wall modifiers

To further test whether misexpressed genes in the *wox13* mutant are transcriptionally regulated by WOX13, we next used dexamethasone (DEX)–dependent system to analyze the expression of candidate target genes upon WOX13 induction. We introduced the *gWOX13-GLUCOCORTICOID RECEPTOR* (*GR*) construct into the *wox13* mutant and first confirmed that the DEX-induced WOX13-GR proteins functionally complement the mutant phenotype (Fig. 3, A and B). Using the *gWOX13-GR* line, we analyzed the expression of candidate genes upon DEX treatment in callus tissues on SIM at day 3. We found that shoot meristem regulator genes that are up-regulated in the *wox13* mutant (Fig. 2A), namely, *WUS*, *STM*, *ESR2*, and *CUC1*, were down-regulated within 24 hours upon DEX treatment (Fig. 3C). This result supports the idea that WOX13 transcriptionally suppresses these genes. As expected from the expression data in the *wox13* mutant, the expression of *ESR1* and *CUC2* was not affected by WOX13 induction (Fig. 3C). We therefore assume that WOX13 specifically represses a subset of genes that regulate shoot fate acquisition. On the other hand, we detected a strong transcriptional up-regulation of *EXPA17* and *MAN7* within 6 hours upon induction and significant induction of *EXPB3* later in 24 hours (Fig. 3D). Our previously reported chromatin immunoprecipitation sequencing (ChIP-seq) data showed that *gWOX13-GFP* directly binds *EXPA17*, *MAN7*, and *EXPB3* loci (*21*), suggesting that WOX13 abruptly up-regulates these cell wall modifier genes via direct physical binding to these loci. Together, WOX13 transcriptionally represses a specific subset of shoot meristem regulators while it directly induces cell wall modifier genes that are potentially involved in cell expansion and cellular differentiation.

scRNA-seq revealed the composition of heterogeneous callus cell population

Cytological analyses and bulk RNA-seq data prompted us to hypothesize that WOX13 may regulate cellular fate control in callus cell population during incubation on SIM. Cellular repertory of SIM-incubated callus remained poorly characterized even in WT; thus, we started with generating a catalog of the callus cells undergoing SAM formation on SIM at day 7 using scRNA-seq. We chose the developmental stage when cytological differences become evident between the genotypes. Considering that callus undergoing shoot regeneration contains large cells, we adopted a plate-based platform, which has a less stringent cellular size limit than commonly adopted droplet-based platforms. We collected protoplasts isolated from callus on SIM at day 7 into 384-well plates using fluorescence-activated cell sorting (FACS) or cellenONE and then subjected the isolated cells to Quartz-Seq2 analysis (*26*). Quartz-Seq2 outperformed other platforms in a benchmarking study using mammalian cells (*27*), yet it has not been applied for plant cells as far as we are aware of. With the criteria of 2000 genes cutoff, we obtained gene expression dataset from 3987 cells combining WT and the *wox13* mutant and detected 8374 genes per cells (fig. S6A and table S4).

We first analyzed the obtained scRNA-seq data from WT and the *wox13* mutant collectively. Principal components analysis and

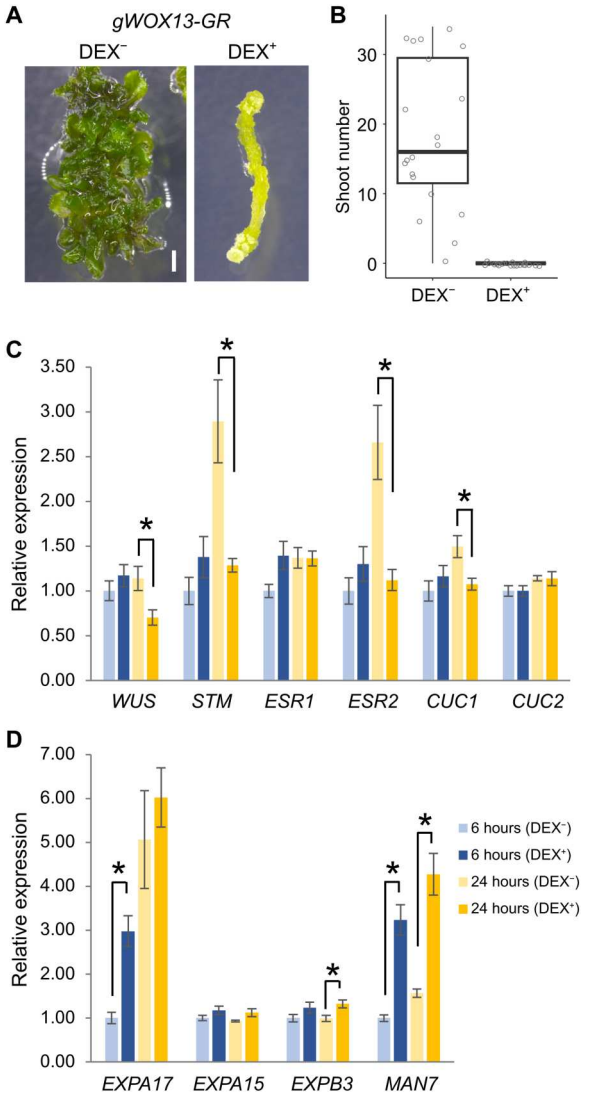

Fig. 3. WOX13 suppresses the expression of shoot meristem regulators and induces cell wall modifiers. (**A** and **B**) Shoot regeneration phenotype of *gWOX13-GR* with DEX (DEX$^+$) or without DEX (DEX$^-$) application during tissue culture. Scale bar, 1 mm. Representative images of explants (A) and quantitative data of shoot number per explant on SIM at day 11 (B). (**C** and **D**) Reverse transcription quantitative polymerase chain reaction analysis of shoot meristem regulators (C) and cell wall modifiers (D) upon WOX13 induction by DEX application. *gWOX13-GR* hypocotyl explants were transferred to +DEX or −DEX SIM media on SIM at day 3 and analyzed at 6 or 24 hours after the transfer. Data are means ± SE (n = 4, biological replicates). Asterisks indicate significant differences based on t test ($P < 0.05$).

unsupervised analyses of the sequencing data uncovered 19 distinct clusters (Fig. 4A). We were able to annotate some of the clusters on the basis of the expression of known marker gene (fig. S6B and Fig. 4, A and B). For instance, clusters 1, 9, and 16 correspond to shoot apices, considering that cells in these clusters display characteristic expression of SAM marker genes, *STM*, *WUS*, and *CLAVATA3* (*CLV3*) and leaf primordia marker genes including *FILAMENTOUS FLOWER* (*FIL*). More specifically, cluster 9 corresponds to the epidermal cell layer of SAM and leaf primordia because L1 marker genes *ARABIDOPSIS THALIANA MERISTEM LAYER 1* (*ATML1*) and *LIPID TRANSFER PROTEIN 6* (*LTP6*) are specifically expressed. Our confocal laser scanning microscopy imaging confirmed that the *pATML1::NLS:3xEGFP* (*28*) signal was specifically detected in the L1 layer of promeristems (Fig. 4C). The cluster 1 appears to consist of L3 layers of SAM, considering that *WUS* and *CLV1* are preferentially expressed, whereas *ATML1* or *FIL* are scarcely expressed. The cluster 16 likely corresponds to the inner layer of leaf primordia cells because these cells are negative for *WUS* and *ATML1* and positive for *FIL* (Fig. 4, A and B). Accordingly, the continuum from the cluster 9 to 16 likely corresponds to the developmental trajectory from SAM to leaf primordia. Other evident clusters were those composed of proliferating cells. It is commonly observed in scRNA-seq data that proliferating cells constitute independent clusters based on their characteristic gene expression profile (*18*). S phase marker genes including *HISTONE H4* (*HIS4*) and *TSO2* were mainly expressed in clusters 3 and 18, whereas G_2-M phase marker genes such as *CYCB1;2* and *CYCA1;1* were expressed in clusters 11, 14, and 16 (Fig. 4, A and B). Therefore, the loop on the uniform manifold approximation and projection (UMAP) plot consisted of clusters 3, 11, and 14 represents the cluster of proliferating cells. We confirmed that the expression of *pCYB1:2YFP-dBox-YFP* (*29*) was preferentially detected in population of compact calli composed of small polygonal cells (Fig. 4C).

While we were able to infer cellular identity or cellular status of these above-described clusters, it was not obvious for other clusters. We thus generated GFP reporters of the markers and analyzed the spatial expression of each gene. Cambium marker genes, *TDIF RECEPTOR* (*TDR*) and *ARABDOPSIS THALIANA HOMEODOMAIN 8* (*ATHB8*), which are strongly enriched in the right half of the UMAP plot, were mainly detected in the inner layers of the callus (Fig. 4C). This observation suggests that the right half of the UMAP plot corresponds to the inner cell layers and the left half to the outer layers of the callus. We should also note that *ATHB8* signal was additionally detected in promeristems, which is consistent with scRNA-seq data that subpopulation of cells in the cluster 1 also express *ATHB8* (Fig. 4C). The observation that the division of the inner and outer cell layers coincides with the primary axis in the UMAP plot indicates that the primary parameter that accounts for the major difference in gene expression profile is the cellular location along the outer-inner layer axis.

Within the outer layers cell population or the left half of the UMAP plot, clusters located in the bottom half correspond to SAM and emerging leaf primordia as described above (Fig. 4A), whereas the clusters in the top half were not well characterized on the basis of the listed marker genes. However, cell image data obtained during protoplast disposal showed that cells in clusters 5, 12, and 17 have longer diameters (fig. S6C). Our imaging analyses revealed that a marker gene of cluster 12, *EXPA17*, was specifically detected in expanded globular cells located in the outer layers of the callus (Fig. 4C). Likewise, *GAST1 PROTEIN HOMOLOG 5* (*GASA5*), which is preferentially expressed in cluster 5, 12, and 17 displayed similar expression pattern in expanded cells in the outer layers, further confirming the observation (Fig. 4C). Cluster 17 has a gene expression profile that is largely distinct from other clusters, which has a higher number of cluster-specific marker genes. Marker genes *CELLULASE 5* (*CEL5*) and α-β *HYDROLASE* have a specific expression in a subpopulation of highly expanded globular cells (Fig. 4). Together, we find that the global gene expression

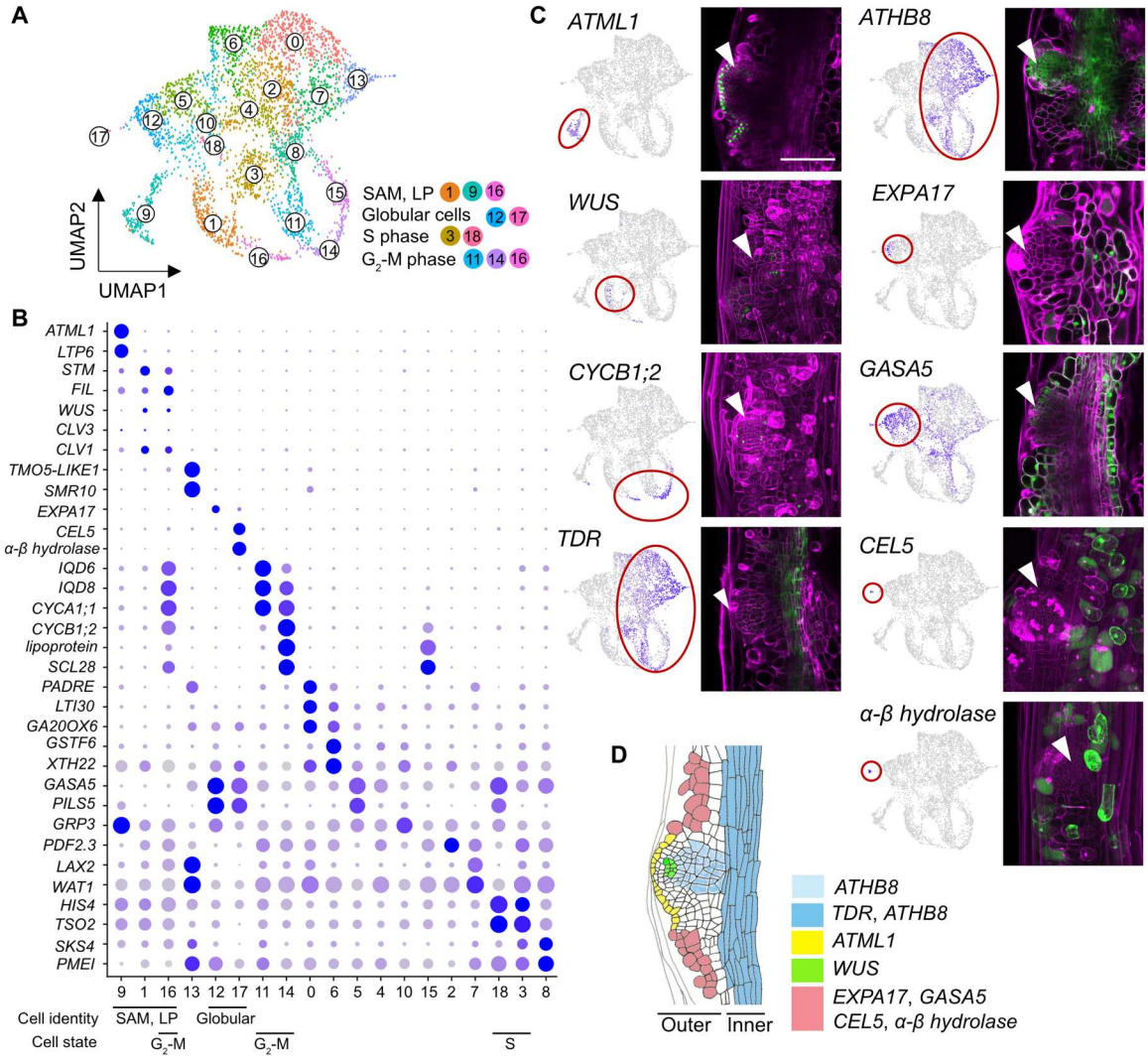

Fig. 4. scRNA-seq revealed the composition of heterogeneous callus cell population. (**A**) UMAP plot of the scRNA-seq dataset analyzing 3987 isolated protoplast cells from SIM at day 7. Clusters representing SAM, LP (leaf primordia), highly expanded globular cells, and proliferating cells in S phase and G_2-M phase are annotated. (**B**) Dot blot visualization of genes listed as markers of clusters. (**C**) Reporter GFP expression of each gene in callus undergoing meristem initiation on SIM at day 7. Arrowheads indicate promeristems or SAMs. Red circles highlight specific cluster(s) for gene expression. Scale bar, 0.1 mm. (**D**) A schematic illustration of the spatial expression pattern of marker genes.

profile is firstly divided into inner and outer layers of the callus, and then, the cells in the outer layers are further divided into SAM and non-meristematic cells (Fig. 4D).

Cellular composition of the callus is modified in the *wox13* mutant

To test whether *wox13* mutant displays differential cellular composition, we next separately analyzed WT and the *wox13* mutant data. As expected from the morphological phenotype of enhanced shoot regeneration, cells in clusters 1, 9, and 16 (SAM and leaf primordia) were highly enriched in the *wox13* mutant (Fig. 5A). For instance, the proportion of *ATML1* expression cells was higher in the *wox13* mutant (10.1% in *wox13* versus 1.6% in WT). We confirmed higher abundance of *ATML1*-positive cells in the *wox13* mutant on SIM at day 7 by imaging *pATML1::NLS:3xEGFP* (Fig. 5B), although the difference in *ATML1* expression was not prominent at an earlier time point on SIM at day 3. This is consistent with our bulk RNA-seq data showing that the *ATML1* expression was unaffected in the *wox13* mutant on SIM at day 4 (Fig. 2A).

We next compared the spatial expression pattern of *WUS* using *gWUS-GFP*$_3$ (*30*). As expected from the accelerated SAM formation, we observed larger foci of *WUS*-expressing cells on SIM at day 7 in the *wox13* mutant. Notably, we found that the number of cells expressing *WUS* was higher in the *wox13* mutant calli at the early stage of incubation, SIM at day 3 (Fig. 5C), when neither callus morphology nor callus size measured by its projection area was significantly affected in the *wox13* mutant (fig. S7, A and B). *WUS* transcription is directly induced by cellular cytokinin response (*7*); we thus tested the possibility that cytokinin response is elevated in *wox13* mutant. We compared the expression of cytokinin reporter *TCSn::GFP* (*31*), but we did not detect any difference in the expression level or the spatial pattern of *TCSn::GFP* between WT and the *wox13* mutant

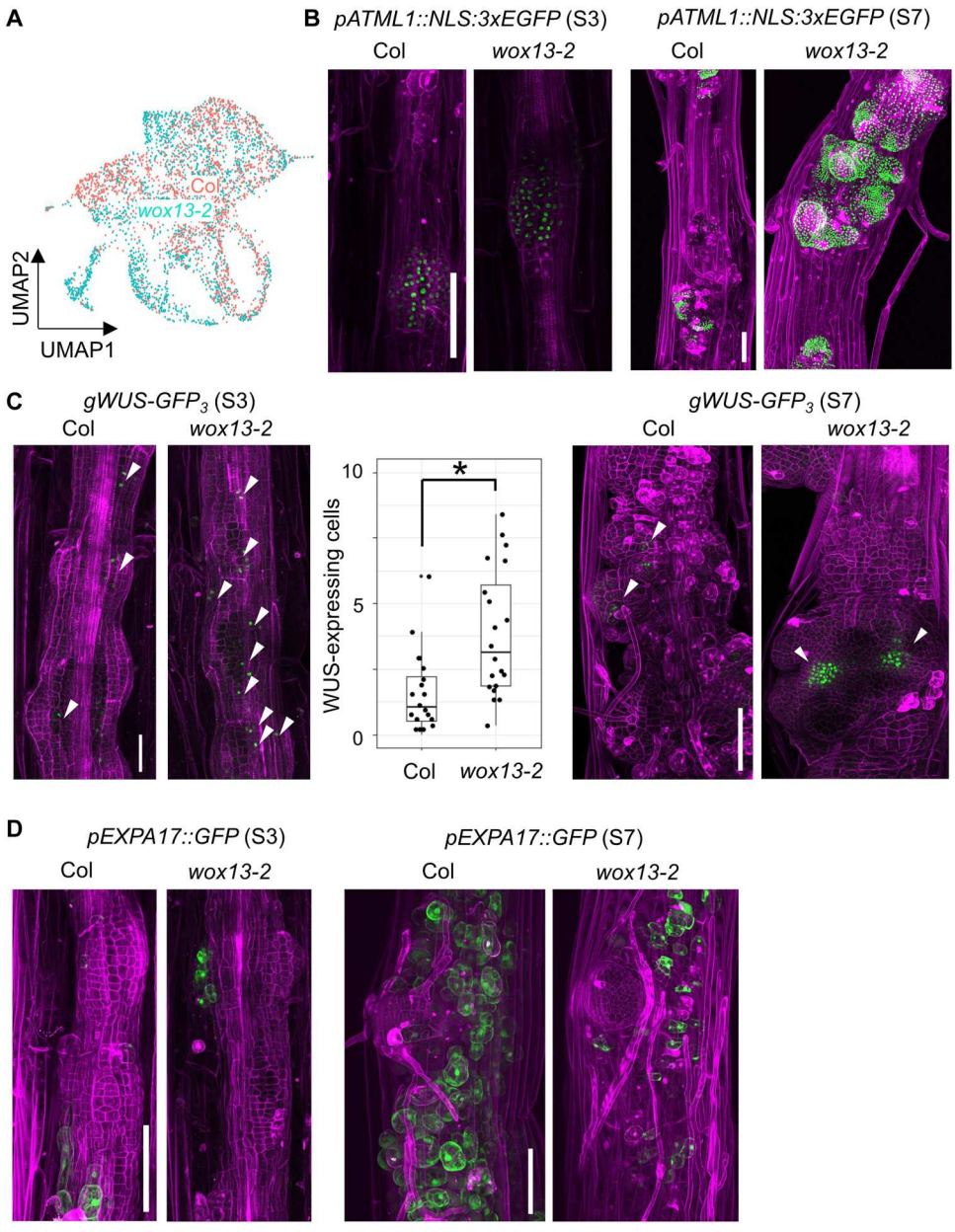

Fig. 5. Differential callus cell composition between WT and the *wox13* mutant. (**A**) UMAP plot of the scRNA-seq dataset describing the differential cellular composition of callus cells depending on genotypes. (**B** to **D**) Reporter GFP expression of *ATML1* (B), *WUS* (C), and *EXPA17* (D) on SIM at day 3 (S3) or SIM at day 7 (S7). Arrowheads indicate GFP-positive cells. Scale bars, 0.1 mm.

(fig. S7C). In addition, the GO category "response to cytokinin" was not significantly enriched in DEG in our bulk transcriptome dataset ($P = 0.13$ on SIM at day 4 and $P = 0.23$ on SIM at day 7). These data together suggest that the observed difference in *WUS* expression is more likely due to the primary output of gene regulatory control by WOX13 rather than an indirect consequence of earlier progression of meristem formation or modified hormone response.

On the other hand, we detected cell types where WT cells were more highly abundant. The relative proportion of *EXPA17*-positive cells was higher in WT (4.7%) than in *wox13* (0.8%). *EXPA17* was expressed in few callus cells on SIM at day 3 in both genotypes, and *EXPA17*-expressing cells increased by SIM at day 7 specifically in WT (Fig. 5D). These observations are consistent with our cytological analyses that highly expanded globular cells are mostly missing in the *wox13* mutant. Collectively, our comparative scRNA-seq analyses followed by imaging of cell type marker genes revealed that the differential expression between WT and *wox13* mutant is at least partly attributable to the difference in cellular composition of the callus.

Mutually repressive WOX13 and WUS demarcate callus cell identity

Our data described above indicate that WOX13 promotes non-meristematic cell fate in callus. Previous studies have established WUS

as a key regulator that specifies cellular fate to become SAM (*7*, *8*, *32*), leading us to hypothesize that WOX13 and WUS may serve as binary cell fate determinants in pluripotent callus cell populations. To explore regulatory relationships between WOX13 and WUS, we first analyzed the spatiotemporal expression of WOX13 and WUS by simultaneously visualizing them with mRUBY and GFP, respectively. *gWOX13-mRUBY* signal was broadly observed in callus with sporadic spots of weak expression, consistent with the observation using *gWOX13-GFP* (Fig. 1). We observed that the *gWUS-GFP*$_3$ expression often initiates in these WOX13-negative spots (18 of 22; Fig. 6A). Alternatively, we also observed minor cases where *gWUS-GFP*$_3$ and *gWOX13-mRUBY* expression is overlapped at an early stage of *WUS* expression (4 of 22; Fig. 6B). Serial imaging analysis revealed that even in cases of initial coexpression, the expression domains of *WOX13* and *WUS* gradually become spatially separated, and *WOX13* is totally absent from promeristems (Fig. 6C) and the established SAM (Fig. 6, D and E).

The establishment of a mutually exclusive spatial expression pattern raises the possibility that WOX13 and WUS may inhibit each other. As described earlier, we find that *WUS* expression is elevated in the *wox13* mutant (Figs. 2B and 5C), and WOX13 transcriptionally represses *WUS* in vivo (Fig. 3C). We also tested the regulatory role of WOX13 on the promoter activity of *WUS* using a transactivation assay using the luciferase reporter. As shown in Fig. 7A, overexpression of WOX13 significantly suppressed the promoter activity of *WUS* in *Arabidopsis* culture cells, underscoring the idea that WOX13 negatively regulates *WUS* expression. Using transactivation assay, we next tested the transcriptional regulation of WUS on *WOX13* promoter and found that the overexpression of WUS strongly suppresses the promoter activity of *WOX13* (Fig. 7B). Furthermore, ChIP data described in a previous study (*33*) showed that WUS physically binds *WOX13* locus (Fig. 7C).

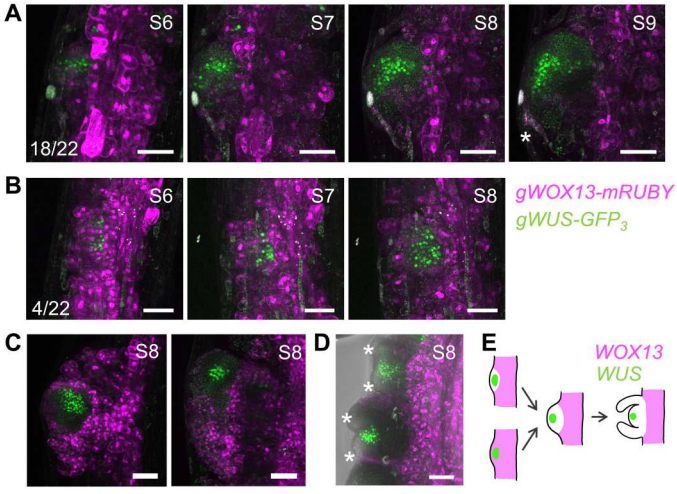

Fig. 6. Spatial separation of WOX13 and WUS expression domains. (**A** and **B**) Live imaging of *gWOX13-mRUBY* (magenta) and *gWUS-GFP*$_3$ (green). Representative cases from two types of relative expression pattern are shown. Consecutive observation was performed daily from SIM at day 6 (S6) to SIM at day 8 (S8) or SIM at day 9 (S9). (**C** and **D**) Snapshot image of *gWOX13-mRUBY* (magenta) and *gWUS-GFP*$_3$ (green) in promeristems (C) and SAM (D). Asterisks show leaf primordia. Scale bars, 50 μm. (**E**) A schematic illustration of the spatial expression pattern of WOX13 and WUS.

These data together demonstrate that WOX13 and WUS reciprocally inhibit the expression of each other.

To test whether the up-regulation of *WUS* expression is relevant for the enhanced shoot regeneration phenotype of the *wox13* mutant, we analyzed the genetic interactions between *WUS* and *WOX13*. We found that enhanced shoot regeneration of *wox13* is totally suppressed by incorporating *wus* mutation (Fig. 7D) (*34*). We therefore conclude that *wus* mutation is epistatic to *wox13* mutation in the control of shoot regeneration, which is in line with the regulatory mechanisms that WOX13 suppresses *WUS*. We also noted that another aspect of *wox13* mutant phenotype, namely, the lack of highly expanded globular cells, is not recovered by introgressing *wus* mutation (Fig. 7D). These observations suggest that the enhanced shoot regeneration phenotype of the *wox13* mutant is dependent on *WUS* repression, whereas the formation of highly expanded globular cells is independent on *WUS*.

DISCUSSION

In this study, we found a previously unappreciated regulatory layer on shoot regeneration that mediates cell fate control. Unlike other known negative regulators of shoot regeneration such as PRC2 or MET1 that prevent cellular identity shift from callus toward SAM, WOX13 negatively affects shoot regeneration efficiency by promoting the acquisition of alternative cell fate to become highly expanded globular cells. WOX13 directly induces the expression of *EXPs* and *MAN7* that are likely involved in cell expansion and cellular differentiation (*35*, *36*) while negatively regulating shoot meristem regulators such as *WUS*, *STM*, *ESR2*, and *CUC1*. WOX13 constitutes a mutually repressive regulatory circuit with WUS, thereby spatially separating micro territories within the callus cell population. (Fig. 7E).

This study sheds light on a long-standing question of how callus cell fates are determined. A recent study revealed that the cells in middle layers of callus on CIM have pluripotency, which are later incorporated into SAMs (*6*). Our scRNA-seq dataset is in line with that study in that the positional information along the outer-inner axis is primarily important for determining the cellular fate. In this study, we propose that cells in outer layers are secondarily specified into promeristems or other cell types including highly expanded globular cells. Our data suggest that the second-step fate specification is mediated by the two reciprocally inhibiting WOX transcription factors, i.e. WUS promotes SAM formation and WOX13 promotes the formation of highly expanded globular cells. Given that WOX13 expression is induced by auxin and WUS suppresses cellular auxin response, the regulatory relationship constitutes a coherent mutual repression (Fig. 7E). Mutually repressive regulation between WUS and WOX13 likely avoid intermediate cellular status, as reported in other binary cellular identity specification mechanisms such as adaxial and abaxial fate of leaf cells (*37*). Noteworthy, we observe a domain of cell population where neither *WUS* nor *WOX13* is expressed at later stage of SAM establishment (Fig. 6C). The *gWUS-GFP*$_3$ reporter line used in this study reflects the promoter activity of *WUS*, while WUS protein is reported to be mobile via plasmodesmata in SAM (*38*). Therefore, it is possible that WUS protein spreads to surrounding cells and represses *WOX13* expression. Potential roles of the mobility of transcription factor(s) in controlling callus cell fates would be an interesting topic for future studies.

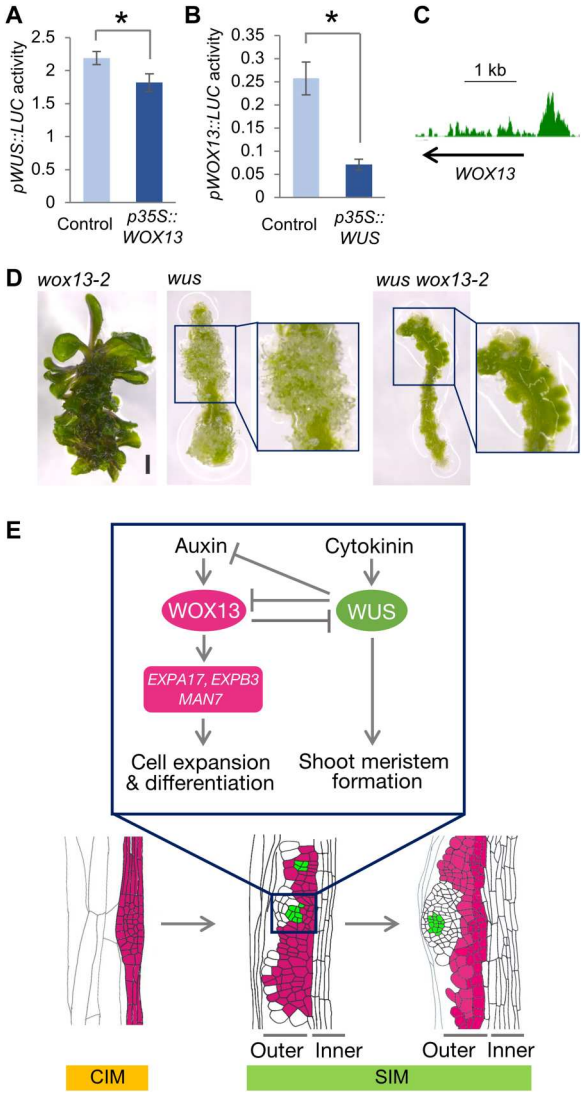

Fig. 7. Mutually repressive WOX13 and WUS demarcate callus cell identity. (**A** and **B**) Reporter luciferase assay to analyze *WUS* promoter activity upon WOX13 overexpression (A) and *WOX13* promoter activity upon WUS overexpression (B). Data are means ± SE [n = 9 in (A) and n = 3 in (B), biological replicates]. (**C**) ChIP-seq data showing *WUS-mCherry* binding to *WOX13* locus. The data are retrieved from a previous report (*33*). (**D**) Genetic interaction between *wox13* and *wus*. Representative image of the explant on SIM at day 21 are shown. Scale bar, 1 mm. (**E**) A schematic diagram describing WOX13 function in the control of callus cell fate and its relationships with WUS. The top panel summarizes the regulatory scheme, and the bottom panel describes the spatiotemporal expression pattern of WOX13 (magenta) and WUS (green).

A recent study showed that only a subset of WUS-expressing cells eventually become SAMs and coexpression of PIN1 and CUC2 is deterministic for the SAM fate (*9*). We assume that cell fate determination to become SAM is a multistep processes, and the PIN1-CUC2–mediated process acts later than the WOX13-WUS–dependent process. In addition, CLV3 negatively regulates *WUS* to maintain the SAM homeostasis (*39*). Potential relationships between CLV3 and WOX13 have not been examined, yet they are unlikely relevant considering that *CLV3* is expressed at a later stage of SAM establishment (*8*) when WOX13 is already shut-off in the meristem region. Newly established SAMs from calli were not larger in the *wox13* mutant with comparable WUS-expressing domain (fig. S8), further supporting the hypothesis that WOX13 is not involved in the later stage of SAM formation. Considering that shutting down WOX13 is a key step in meristem establishment, how WOX13 expression is repressed during incubation on SIM is an important question. Although WUS apparently plays roles in repressing *WOX13*, WUS alone does not sufficiently account for the spatial expression pattern of WOX13 in calli. We previously found that cytokinin application does not affect *WOX13* transcription (*22*), and further analyses are highly awaited to uncover regulatory mechanisms to fine-tune the spatial pattern of *WOX13* expression.

Moreover, Quartz-Seq2 allowed us to establish a high-quality cell atlas of heterogeneous cell population of SIM-incubated callus. We successfully detected the expression of key developmental regulators, such as *WUS* and *CLV3*, which have been difficult to detect by high-throughput scRNA-seq analyses using other platforms (*18*). Quartz-Seq2 won the top score in the benchmarking report using mammalian cells among high-throughput scRNA-seq platforms (*27*). The outstanding sensitivity to detect a large number of genes makes Quartz-Seq2 an attractive option in plant science as well, especially when working with cell types with little prior information. Although cellular heterogeneity of callus has been well recognized at the cytological level, callus cell types have not been characterized in terms of gene expression profile or physiological roles. Lack of cell type marker genes prevented us from performing cell type–specific transcriptome analyses, which have been long applied to other tissues such as roots (*40*). Our scRNA-seq dataset offers a useful starting point for the full description of the callus cell population undergoing shoot regeneration. Regulatory mechanisms mediated by WOX13 and WUS only partially account for the specification of the identified cell types, and further studies are needed to fully unveil specification mechanisms of the remaining cell types. Furthermore, additional scRNA-seq analyses at earlier incubation stages are expected to decipher cell fate specification processes at higher resolution.

This study together with our recent report revealed a specific regulation on diverse regenerative responses. Whereas WOX13 is a negative regulator of de novo shoot formation, it is indispensable for tissue repair and organ reconnection (*21*, *22*). Considering that the tissue repair and the de novo organogenesis involve largely distinct cellular processes, it is reasonable to assume that plants need to activate specific responses in a context-dependent manner in physiological conditions. This specific regulation by WOX13 contrasts with WIND1, which generally promotes various aspects of regeneration (*11*, *41*, *42*). We previously reported that WIND1 transcriptionally induces *WOX13*, which directly activates *WIND2* and *WIND3* expression (*21*). Future studies are awaited to untangle how these regulatory relationships between WINDs and WOX13 control regenerative responses in diverse physiological conditions.

This study also has important implication for agricultural and horticultural applications. Several developmental regulators including WUS, WOX5, and BABY BOOM have been shown to promote shoot regeneration efficiency in crop species when overexpressed (*43*, *44*). Compared to the gain-of-function approach, which typically requires the incorporation of transgenes to plant genomes, loss-of-function strategy has an obvious advantage because transgene-free genome editing is well established in many species.

Loss-of-function mutant of *wox13* does not have severe morphological or developmental defects during normal development (*45*), thus knocking out WOX13 may have a potential for boosting the efficiency of tissue culture–mediated de novo shoot regeneration in crops.

MATERIALS AND METHODS

Plant materials and growth conditions

The WT *Arabidopsis* plants used in this study is Columbia (Col-0). The *wox13-2* mutant was originally in L*er* background and backcrossed to Col-0 three times (*45*). We used the *wus* mutant (SAIL_150_G06) for phenotypic analyses and *gWUS-GFP*$_3$ (*30*), *gWOX13-GFP* (*21*), *pWOX5::ER-GFP* (*24*), *pATML1::NLS:3xEGFP* (*28*), *pCYB1:2YFP-dBox-YFP* (*29*), and *TCSn::GFP* (*31*) for imaging analyses. Plants were grown on half-strength Murashige-Skoog (MS) medium containing 0.6% (w/v) Gelzan and 1% (w/v) sucrose under constant light at 22°C. For tissue culture experiments, 7- to 8-mm explants were prepared from 7-day-old etiolated seedlings and precultured on CIM [Gamborg B5 medium containing 0.25% (w/v) Gelzan, 2%(w/v) glucose, 2,4-D (0.5 mg/liter), and kinetin (0.1 mg/liter)] for 4 days before subsequent incubation on SIM [Gamborg B5 medium containing 0.25% (w/v) Gelzan, 2%(w/v) glucose, indole-3-acetic acid (0.15 mg/liter), and 2-iPA (0.5 mg/liter)] under constant light at 22°C.

Generation of transgenic plants

To visualize the spatiotemporal expression, 1.2- to 2-kb promoters of *EXPA17*, *GASA5*, *CEL5*, *ALPHA-BETA HYDROLASE*, *TDR*, and *ATHB8* were cloned in pDONRp4-p1R by Gateway BP cloning (Invitrogen). Promoter of each gene was amplified using primers listed below: EXPA17-pro-F (5′-TATAATGTGGGGTATATTTTGTC-3′) and EXPA17-pro-R (5′-TTTGTTTTCTTTCAATTTCTTAGG-3′) for *EXPA17* (AT4G01630); GASA5-pro-F (5′-CCTAAGTTCGTTTCTCGATAA-3′) and GASA5-pro-R (5′-AAACAATAAAACGGATTAAAGA-3′) for *GASA5* (AT3G02885); CEL5-pro-F (5′-CCCTCGAGTTCTTAAGGTAC-3′) and CEL5-pro-R (5′-TCTTGTTATTGTGTTGGCTTGAG-3′) for *CEL5* (AT1G22880); Alpha-beta-pro-F (5′-GTTGGAATGACTAGAATTTC-3′) and Alpha-beta-pro-R (5′-GGCTCAACAAAAGCTTAGAGAG-3′) for *ALPHA-BETA HYDROLASE* (AT4G24140); TDR-pro-F (5′-GGTTCTTCCACTACATCACG-3′) and TDR-pro-R (5′-CGTAGCTTTTAGAAAGAAATTAAAG-3′) for *TDR* (AT5G61480); and ATHB8-pro-F (5′-CTTATCACAGGGGACAATGTCG-3′) and ATHB-pro-R (5′-CTTTGATCCTCTCCGATCTCTC-3′) for *ATHB8* (AT4G32880). After verifying the full-length sequence of the cloned fragment, the promoter together with pDONR-L1-GFP-L2 was transferred to the binary vector R4pGWB501 (*46*) via an LR reaction (Invitrogen). For the generation of *WOX13* (AT4G35550) genomic fusion lines, *gWOX13-mRUBY* and *gWOX13-GR* were constructed in the same way with *gWOX13-GFP* as described before (*21*). For plant transformation, the binary vectors carrying transfer DNA (T-DNA) were introduced into *Agrobacterium tumefaciens* strain GV3101 by electroporation, and the resultant bacteria were infiltrated into Col-0 plants by the floral dip method. For comparative expression analyses, the transgenic lines harboring the single insertions were introgressed into *wox13-2* mutants, and the homozygous plants were subjected to imaging analyses.

Imaging analysis

For snapshot observations, explants were stained using propidium iodide (PI) [100 μg/ml (day 0; CIM at day 1), 40 μg/ml (CIM at day 4), and 20 μg/ml (SIM at days 3, 4, and 7); Invitrogen] for 30 min and imaged by SP8 (Leica) using a 488-nm laser for GFP and PI and 561-nm laser for mRUBY. For live imaging, explants on SIM at day 6 were transferred to the 35-mm glass-bottom dish (Matsunami), covered by a 7-mm-thick SIM and imaged under SP8.

Quartz-Seq2–based scRNA-seq

We prepared two biological replicates for scRNA-seq analysis (fig. S9A). A total of 170 to 195 hypocotyl explants for each genotype (Col and *wox13-2*), which have been incubated on CIM for 4 days and then additionally incubated on SIM for 7 days, were treated with digestion buffer [600 mM mannitol, 2 mM $MgCl_2$, 0.1% bovine serum albumin, 2 mM $CaCl_2$, 2 mM MES, 10 mM KCl, 1.5% Cellulase RS, and 0.1% Pectolyase (pH 5.5)] for 1 hour at room temperature as described before (*47*). The protoplast solution was strained through a 70-μm filter. The filtered solution was centrifuged at 200*g* for 6 min and then washed once and lastly strained through a 40-μm filter. The protoplast pellet was resuspended in 0.5 ml of resuspension buffer. Cell viability was confirmed by PI staining. Alive singlet cells were captured by BD FACSAria II SORP (BD Biosciences, NJ, USA; fig. S9B) or cellenONE (Cellenion, Lyon, France) and collected into eight 384-well plates for each platform. Sequence library preparation of Quartz-Seq2 was performed for scRNA-seq analysis according to the previous study (*26*), and the libraries were sequenced by an Illumina NextSeq 500 High Output Kit v2.5 (75 cycles; Illumina, CA, USA). In calculation for digital expression matrix, we used genome file and annotation gtf file, which was provided by B. Cole (*48*). Flow cytometer information obtained from FACS and cell analysis data from cellenONE were analyzed together with the digital expression matrix. Cell analysis data obtained from cellenONE includes diameter information per isolated cell. Seurat v3.1.4 was used for the downstream data analyses including filtering, dimension reduction, cell clustering, and identification of marker genes. The UMI expression matrix with cells expressing at least 2000 genes was loaded into Seurat (Fig. 4A). A total of 3987 cells (1898 cells for WT and 2089 cells for *wox13* mutant) with an average of 8373 genes were used for the following analyses. The dimensions of the expression matrix were then reduced by the RunPCA function, and the top 15 dimensions were used for FindNeighbors function and UMAP analysis. The cell clusters were identified by the FindClusters function with a resolution of 0.7. Marker genes for each cluster were identified using FindAllMarkers function. Because there was no obvious batch effect between biological replicates (fig. S9C), we did not perform the integration process.

RNA extraction for bulk RNA-seq

To evaluate gene expression in callus, explants were harvested for RNA extraction at the designated time after incubation. Total RNA was extracted using the RNeasy Plant Mini Kit (QIAGEN) according to the manufacturer's instructions. For RNA-seq, isolated total RNA solution was subjected to on-column DNase digestion (QIAGEN) to eliminate genomic DNA contamination.

Bulk RNA-seq data analysis

For the transcriptome comparison, total RNA was prepared from explants. Biological triplicates were prepared for each genotype (Col and *wox13-2*) and time point (day 0; CIM at day 4, SIM at day 4, and SIM at day 7). Isolated total RNA was subjected to library preparation using the KAPA Stranded mRNA-Seq Kit (Kapa Biosystems) with NEBNext Multiplex Oligos for Illumina (New England Biolabs) used as adapters and Agencourt AMPure XP (Beckman Coulter) beads in place of KAPA Pure Beads. Single-end sequencing was performed using the Illumina NextSeq500 platform. Raw data files (bcl format) were converted to fastq files by bcl2fastq (Illumina). On average, 92% (81 to 95%) of reads were mapped to the *Arabidopsis* TAIR10 reference transcript model using the RSEM package (*49*) with default parameters. Differentially expressed transcripts between genotypes at each time points were identified using the edgeR package in R/Bioconductor with FDR < 0.01 cutoff. GO analysis was performed using the clusterProfiler package (3.18.1) (*50*), and the obtained GO category list was simplified using "simplify" function.

Reverse transcription quantitative polymerase chain reaction

To evaluate gene expression following DEX induction, 17 hypocotyl explants were harvested for RNA extraction. Total RNA was extracted using the RNeasy Plant Mini Kit (QIAGEN) according to the manufacturer's instructions. Total RNA (400 ng) was then subjected to the first-strand cDNA synthesis with PrimeScript RT reagent kit (Takara). Quantitative real-time polymerase chain reaction (PCR) was performed in technical duplicates using the THUNDERBIRD SYBR qPCR Mix (Toyobo) with the primers described below. Relative transcript quantities were calculated using standard curves for each primer set and values normalized to an internal control gene, *PROTEIN PHOSPHATASE 2A SUBUNIT A3* (*PP2AA3*). For quantification of transcript level of each gene, the listed primers were used: WUS-RT-F (5′-AGCCGATCAGATCCAGAAGA-3′) and WUS-RT-F (5′-AACCGAGTTGGGTGATGAAG-3′) for *WUS* (AT2G17950); STM-RT-F (5′-CCTTACCCTTCGGAGCAACAA-3′) and STM-RT-R (5′-TCCAATGCCGTTTCCTCTGGTTTA-3′) for *STM* (AT1G62360); ESR1-RT-F (5′-ACAGCTGTCATTATGCCTGAACCA-3′) and ESR1-RT-F (5′-GGTAGAGGAATCTAACGGTAGAGA-3′) for *ESR1* (AT1G12980); ESR2-RT-F (5′-GCTGACTTCCATGTCGAAGGA-3′) and ESR2-RT-R (5′-TCTGCTGCATCTTAGCTGAATC-3′) for *ESR2* (AT1G24590); CUC1-RT-F (5′-CAGCAGCAGCAGCGTTCTTT-3′) and CUC1-RT-R (5′-AATGACGGAGGAGGAGGAAGAA-3′) for *CUC1* (AT3G15170); CUC2-RT-F (5′-GAGCACGTGTCCTGTTTCTC-3′) and CUC2-RT-F (5′-GTTTCTAGAAACGAAACGAGG-3′) for *CUC2* (AT5G53950); EXPA17-RT-F (5′-GGTCGCAATGATCTTCTCCAC-3′) and EXPA17-RT-F (5′-GGTTTCCATAACCACAAGCTCC-3′) for *EXPA17*; EXPA15-RT-F (5′-CTTGGTGACCAATGTTGGTG-3′) and EXPA15-RT-F (5′-CCATCACTAGCAGTCACCTT-3′) for *EXPA15* (AT2G03090); MAN7-RT-F (5′-CGTCACGGTTCACTCTTACC-3′) and MAN7-RT-F (5′-GTGAAGAACGTTCTGTGCGT-3′) for *MAN7* (AT5G66460); and PP2AA3-RT-F (5′-GACCAAGTGAACCAGGTTATTGG-3′) and PP2AA3-RT-R (5′-TACTCTCCAGTGCCTGTCTTCA-3′) for *PP2AA3* (AT1G13320).

Transactivation assay

Transactivation assay was performed as described previously (*11*). The *p35S::NOS terminator* vector was used as control. The *pWOX13::L-LUC* vector was used as a reporter, and the *p35S::R-LUC* was used as an internal control. To construct *p35S::WOX13* and *p35S::WUS*, CDS of *WOX13* and *WUS* was amplified, cloned into pDONR221, and transferred to pUGW2 (*51*) by Gateway LR cloning (Invitrogen). To construct *pWOX13::LUC* and *pWUS::LUC*, promoter of *WOX13* and *WUS* was amplified, cloned into pDONRp4p1R, and transferred to R4L1pUGW35 (*51*) by LR cloning. Particle bombardment was performed using the Biolistic PDS-1000/He system (Bio-Rad), and luciferase assay was performed using the Dual-Luciferase Reporter Assay System (Promega). *Arabidopsis* MM2d cultured cells were used as host cells, and luciferase activities were quantified using the Mithras LB940 Microplate Luminometer (Berthold Technologies).

Supplementary Materials

This PDF file includes:
Figs. S1 to S9
Legends for tables S1 to S4

Other Supplementary Material for this manuscript includes the following:
Tables S1 to S4

View/request a protocol for this paper from *Bio-protocol*.

REFERENCES AND NOTES

1. K. D. Birnbaum, A. S. Alvarado, Slicing across kingdoms: Regeneration in plants and animals. *Cell* **132**, 697–710 (2008).
2. M. Ikeuchi, D. S. Favero, Y. Sakamoto, A. Iwase, D. Coleman, B. Rymen, K. Sugimoto, Molecular mechanisms of plant regeneration. *Annu. Rev. Plant Biol.* **70**, 377–406 (2019).
3. D. Valvekens, M. Van Montagu, M. Van Lijsebettens, *Agrobacterium tumefaciens*-mediated transformation of *Arabidopsis thaliana* root explants by using kanamycin selection. *Proc. Natl. Acad. Sci. U.S.A.* **85**, 5536–5540 (1988).
4. K. Sugimoto, Y. Jiao, E. M. Meyerowitz, Arabidopsis regeneration from multiple tissues occurs via a root development pathway. *Dev. Cell* **18**, 463–471 (2010).
5. A. Kareem, K. Durgaprasad, S. Sugimoto, Y. Du, A. J. Pulianmackal, Z. B. Trivedi, P. V. Abhayadev, V. Pinon, E. M. Meyerowitz, B. Scheres, K. Prasad, PLETHORA genes control regeneration by a two-step mechanism. *Curr. Biol.* **25**, 1017–1030 (2015).
6. N. Zhai, L. Xu, Pluripotency acquisition in the middle cell layer of callus is required for organ regeneration. *Nat. Plants* **7**, 1453–1460 (2021).
7. T.-Q. Zhang, H. Lian, C.-M. Zhou, L. Xu, Y. Jiao, J.-W. Wang, A two-step model for de novo activation of *WUSCHEL* during plant shoot regeneration. *Plant Cell* **29**, 1073–1087 (2017).
8. S. P. Gordon, M. G. Heisler, G. V. Reddy, C. Ohno, P. Das, E. M. Meyerowitz, Pattern formation during de novo assembly of the Arabidopsis shoot meristem. *Development* **134**, 3539–3548 (2007).
9. V. Varapparambath, M. M. Mathew, A. P. Shanmukhan, D. Radhakrishnan, A. Kareem, S. Verma, J. J. Ramalho, B. Manoj, A. R. Vellandath, M. Aiya, R. K. Radha, A. N. Landge, A. P. Mähönen, M. G. Heisler, D. Weijers, K. Prasad, Mechanical conflict caused by a cell-wall-loosening enzyme activates de novo shoot regeneration. *Dev. Cell* **57**, 2063–2080.e10 (2022).
10. Y. Daimon, K. Takabe, M. Tasaka, The CUP-SHAPED COTYLEDON genes promote adventitious shoot formation on calli. *Plant Cell Physiol.* **44**, 113–121 (2003).
11. A. Iwase, H. Harashima, M. Ikeuchi, B. Rymen, M. Ohnuma, S. Komaki, K. Morohashi, T. Kurata, M. Nakata, M. Ohme-Takagi, E. Grotewold, K. Sugimoto, WIND1 promotes shoot regeneration through transcriptional activation of *ENHANCER OF SHOOT REGENERATION1* in Arabidopsis. *Plant Cell* **29**, 54–69 (2017).
12. W. Li, H. Liu, Z. J. Cheng, Y. H. Su, H. N. Han, Y. Zhang, X. S. Zhang, DNA methylation and histone modifications regulate de novo shoot regeneration in *Arabidopsis* by modulating WUSCHEL expression and auxin signaling. *PLOS Gen.* **7**, e1002243 (2011).

13. A. Lambolez, A. Kawamura, T. Takahashi, B. Rymen, A. Iwase, D. S. Favero, M. Ikeuchi, T. Suzuki, S. Cortijo, K. E. Jaeger, P. A. Wigge, K. Sugimoto, Warm temperature promotes shoot regeneration in *Arabidopsis thaliana*. *Plant Cell Physiol.* **63**, 618–634 (2022).
14. D. Coleman, A. Kawamura, M. Ikeuchi, D. S. Favero, A. Lambolez, B. Rymen, A. Iwase, T. Suzuki, K. Sugimoto, The SUMO E3 ligase SIZ1 negatively regulates shoot regeneration. *Plant Physiol.* **184**, 330–344 (2020).
15. E. Shapiro, T. Biezuner, S. Linnarsson, Single-cell sequencing-based technologies will revolutionize whole-organism science. *Nat. Rev. Genet.* **14**, 618–630 (2013).
16. C. Seyfferth, J. Renema, J. R. Wendrich, T. Eekhout, R. Seurinck, N. Vandamme, B. Blob, Y. Saeys, Y. Helariutta, K. D. Birnbaum, B. De Rybel, Advances and opportunities in single-cell transcriptomics for plant research. *Annu. Rev. Plant Biol.* **72**, 847–866 (2021).
17. H. P. Gala, A. Lanctot, K. Jean-Baptiste, S. Guiziou, J. C. Chu, J. E. Zemke, W. George, C. Queitsch, J. T. Cuperus, J. L. Nemhauser, A single-cell view of the transcriptome during lateral root initiation in *Arabidopsis thaliana*. *Plant Cell* **33**, 2197–2220 (2021).
18. T.-Q. Zhang, Y. Chen, J.-W. Wang, A single-cell analysis of the Arabidopsis vegetative shoot apex. *Dev. Cell* **56**, 1056–1074 (2021).
19. S. Otero, I. Gildea, P. Roszak, Y. Lu, V. Di Vittori, M. Bourdon, L. Kalmbach, B. Blob, J. O. Heo, F. Peruzzo, T. Laux, A. R. Fernie, H. Tavares, Y. Helariutta, A root phloem pole cell atlas reveals common transcriptional states in protophloem-adjacent cells. *Nat. Plants* **8**, 954–970 (2022).
20. M. Omary, N. Gil-Yarom, C. Yahav, E. Steiner, A. Hendelman, I. Efroni, A conserved superlocus regulates above- and belowground root initiation. *Science* **375**, eabf4368 (2022).
21. M. Ikeuchi, A. Iwase, T. Ito, H. Tanaka, D. S. Favero, A. Kawamura, S. Sakamoto, M. Wakazaki, T. Tameshige, H. Fujii, N. Hashimoto, T. Suzuki, K. Hotta, K. Toyooka, N. Mitsuda, K. Sugimoto, Wound-inducible WUSCHEL-RELATED HOMEOBOX 13 is required for callus growth and organ reconnection. *Plant Physiol.* **188**, 425–441 (2022).
22. H. Tanaka, N. Hashimoto, S. Kawai, E. Yumoto, K. Shibata, T. Tameshige, Y. Yamamoto, K. Sugimoto, M. Asahina, M. Ikeuchi, Auxin-induced WUSCHEL-RELATED HOMEOBOX13 mediates asymmetric activity of callus formation upon cutting. *Plant Cell Physiol.* **64**, 305–316 (2023).
23. M. D. Robinson, D. J. McCarthy, G. K. Smyth, edgeR: A Bioconductor package for differential expression analysis of digital gene expression data. *Bioinformatics* **26**, 139–140 (2010).
24. I. Blilou, J. Xu, M. Wildwater, V. Willemsen, I. Paponov, J. Friml, R. Heidstra, M. Aida, K. Palme, B. Scheres, The PIN auxin efflux facilitator network controls growth and patterning in Arabidopsis roots. *Nature* **433**, 39–44 (2005).
25. N. C. Chiam, T. Fujimura, R. Sano, N. Akiyoshi, R. Hiroyama, Y. Watanabe, H. Motose, T. Demura, M. Ohtani, Nonsense-mediated mRNA decay deficiency affects the auxin response and shoot regeneration in Arabidopsis. *Plant Cell Physiol.* **60**, 2000–2014 (2019).
26. Y. Sasagawa, H. Danno, H. Takada, M. Ebisawa, K. Tanaka, T. Hayashi, A. Kurisaki, I. Nikaido, Quartz-Seq2: A high-throughput single-cell RNA-sequencing method that effectively uses limited sequence reads. *Genome Biol.* **19**, 29 (2018).
27. E. Mereu, A. Lafzi, C. Moutinho, C. Ziegenhain, D. J. McCarthy, A. Álvarez-Varela, E. Batlle, Sagar, D. Grün, J. K. Lau, S. C. Boutet, C. Sanada, A. Ooi, R. C. Jones, K. Kaihara, C. Brampton, Y. Talaga, Y. Sasagawa, K. Tanaka, T. Hayashi, C. Braeuning, C. Fischer, S. Sauer, T. Trefzer, C. Conrad, X. Adiconis, L. T. Nguyen, A. Regev, J. Z. Levin, S. Parekh, A. Janjic, L. E. Wange, J. W. Bagnoli, W. Enard, M. Gut, R. Sandberg, I. Nikaido, I. Gut, O. Stegle, H. Heyn, Benchmarking single-cell RNA-sequencing protocols for cell atlas projects. *Nat. Biotechnol.* **38**, 747–755 (2020).
28. S. Takada, G. Jürgens, Transcriptional regulation of epidermal cell fate in the *Arabidopsis* embryo. *Development* **134**, 1141–1150 (2007).
29. E. Iwata, S. Ikeda, S. Matsunaga, M. Kurata, Y. Yoshioka, M. C. Criqui, P. Genschik, M. Ito, GIGAS CELL1, a novel negative regulator of the anaphase-promoting complex/cyclosome, is required for proper mitotic progression and cell fate determination in *Arabidopsis*. *Plant Cell* **23**, 4382–4393 (2011).
30. M. R. Tucker, A. Hinze, E. J. Tucker, S. Takada, G. Jürgens, T. Laux, Vascular signalling mediated by ZWILLE potentiates WUSCHEL function during shoot meristem stem cell development in the Arabidopsis embryo. *Development* **135**, 2839–2843 (2008).
31. E. Zürcher, D. Tavor-Deslex, D. Lituiev, K. Enkerli, P. T. Tarr, B. Müller, A robust and sensitive synthetic sensor to monitor the transcriptional output of the cytokinin signaling network in planta. *Plant Physiol.* **161**, 1066–1075 (2013).
32. J. L. Gallois, F. R. Nora, Y. Mizukami, R. Sablowski, WUSCHEL induces shoot stem cell activity and developmental plasticity in the root meristem. *Genes Dev.* **18**, 375–380 (2004).
33. Y. Ma, A. Miotk, Z. Šutiković, O. Ermakova, C. Wenzl, A. Medzihradszky, C. Gaillochet, J. Forner, G. Utan, K. Brackmann, C. S. Galván-Ampudia, T. Vernoux, T. Greb, J. U. Lohmann, WUSCHEL acts as an auxin response rheostat to maintain apical stem cells in Arabidopsis. *Nat. Commun.* **10**, 5093 (2019).
34. S. P. Chatfield, R. Capron, A. Severino, P. A. Penttila, S. Alfred, H. Nahal, N. J. Provart, Incipient stem cell niche conversion in tissue culture: Using a systems approach to probe early events in WUSCHEL-dependent conversion of lateral root primordia into shoot meristems. *Plant J.* **73**, 798–813 (2013).
35. D. J. Cosgrove, Plant expansins: Diversity and interactions with plant cell walls. *Curr. Opin. Plant Biol.* **25**, 162–172 (2015).
36. H. He, M. Bai, P. Tong, Y. Hu, M. Yang, H. Wu, CELLULASE6 and MANNANASE7 affect cell differentiation and silique dehiscence. *Plant Physiol.* **176**, 2186–2201 (2018).
37. T. Tameshige, H. Fujita, K. Watanabe, K. Toyokura, M. Kondo, K. Tatematsu, N. Matsumoto, R. Tsugeki, M. Kawaguchi, M. Nishimura, K. Okada, Pattern dynamics in adaxial-abaxial specific gene expression are modulated by a plastid retrograde signal during Arabidopsis thaliana leaf development. *PLOS Genet.* **9**, e1003655 (2013).
38. R. K. Yadav, M. Perales, J. Gruel, T. Girke, H. Jönsson, G. V. Reddy, WUSCHEL protein movement mediates stem cell homeostasis in the Arabidopsis shoot apex. *Genes Dev.* **25**, 2025–2030 (2011).
39. H. Schoof, M. Lenhard, A. Haecker, K. F. Mayer, G. Jürgens, T. Laux, The stem cell population of Arabidopsis shoot meristems in maintained by a regulatory loop between the *CLAVATA* and *WUSCHEL* genes. *Cell* **100**, 635–644 (2000).
40. K. Birnbaum, D. E. Shasha, J. Y. Wang, J. W. Jung, G. M. Lambert, D. W. Galbraith, P. N. Benfey, A gene expression map of the *Arabidopsis* root. *Science* **302**, 1956–1960 (2003).
41. A. Iwase, N. Mitsuda, T. Koyama, K. Hiratsu, M. Kojima, T. Arai, Y. Inoue, M. Seki, H. Sakakibara, K. Sugimoto, M. Ohme-Takagi, The AP2/ERF transcription factor WIND1 controls cell dedifferentiation in Arabidopsis. *Curr. Biol.* **21**, 508–514 (2011).
42. A. Iwase, Y. Kondo, A. Laohavisit, A. Takebayashi, M. Ikeuchi, K. Matsuoka, M. Asahina, N. Mitsuda, K. Shirasu, H. Fukuda, K. Sugimoto, WIND transcription factors orchestrate wound-induced callus formation, vascular reconnection and defense response in Arabidopsis. *New Phytol.* **232**, 734–752 (2021).
43. K. Lowe, E. Wu, N. Wang, G. Hoerster, C. Hastings, M. J. Cho, C. Scelonge, B. Lenderts, M. Chamberlin, J. Cushatt, L. Wang, L. Ryan, T. Khan, J. Chow-Yiu, W. Hua, M. Yu, J. Banh, Z. Bao, K. Brink, E. Igo, B. Rudrappa, P. M. Shamseer, W. Bruce, L. Newman, B. Shen, P. Zheng, D. Bidney, C. Falco, J. Register, Z. Y. Zhao, D. Xu, T. Jones, W. Gordon-Kamm, Morphogenic regulators *BABY BOOM* and *WUSCHEL* improve monocot transformation. *Plant Cell* **28**, 1998–2015 (2016).
44. K. Wang, L. Shi, X. Liang, P. Zhao, W. Wang, J. Liu, Y. Chang, Y. Hiei, C. Yanagihara, L. Du, Y. Ishida, X. Ye, The gene *TaWOX5* overcomes genotype dependency in wheat genetic transformation. *Nat. Plants* **8**, 110–117 (2022).
45. M. Romera-Branchat, J. J. Ripoll, M. F. Yanofsky, S. Pelaz, The WOX13 homeobox gene promotes replum formation in the *Arabidopsis thaliana* fruit. *Plant J.* **73**, 37–49 (2013).
46. T. Nakagawa, S. Nakamura, K. Tanaka, M. Kawamukai, T. Suzuki, K. Nakamura, T. Kimura, S. Ishiguro, Development of R4 gateway binary vectors (R4pGWB) enabling high-throughput promoter swapping for plant research. *Biosci. Biotechnol. Biochem.* **72**, 624–629 (2008).
47. E. E. Sparks, P. N. Benfey, Tissue-specific transcriptome profiling in Arabidopsis roots. *Methods Mol. Biol.* **1610**, 107–122 (2017).
48. C. N. Shulse, B. J. Cole, D. Ciobanu, J. Lin, Y. Yoshinaga, M. Gouran, G. M. Turco, Y. Zhu, R. C. O'Malley, S. M. Brady, D. E. Dickel, High-throughput single-cell transcriptome profiling of plant cell types. *Cell Rep.* **27**, 2241–2247.e4 (2019).
49. B. Li, C. N. Dewey, RSEM: Accurate transcript quantification from RNA-Seq data with or without a reference genome. *BMC Bioinformatics* **12**, 323 (2011).
50. G. Yu, L.-G. Wang, Y. Han, Q. Y. He, clusterProfiler: An R package for comparing biological themes among gene clusters. *OMICS* **16**, 284–287 (2012).
51. T. Nakagawa, T. Kurose, T. Hino, K. Tanaka, M. Kawamukai, Y. Niwa, K. Toyooka, K. Matsuoka, T. Jinbo, T. Kimura, Development of series of gateway binary vectors, pGWBs, for realizing efficient construction of fusion genes for plant transformation. *J. Biosci. Bioeng.* **104**, 34–41 (2007).

Acknowledgments: We thank Y. Iwayama, K. Ohtawa, K. Fukumoto, and N. Mataga (RIKEN RRD) for technical assistance in Quartz-Seq2 analyses; M. Mouri (RIKEN CSRS) for technical support with plasmid construction and transactivation assay; Y. Ikeda (NAIST) for technical support with tissue culture; and A. Furuta for technical support in bulk RNA-seq analysis. We also thank the Single-cell Omics Laboratory for technical consultation in scRNA-seq analyses, the members of the Laboratory for Bioinformatics Research at the RIKEN Center for Biosystems Dynamics Research, and A. Matsushima and T. Ichikawa for IT infrastructure management. **Funding:** This work was supported by JSPS KAKENHI (17K15146, 19H05670, 20K06712, 20H04894, 20H05431, and 22H04713 to M.I. and 20H03284 and 20H05911 to K.S.), by the JST FOREST Program (JPMJFR214H to M.I.), by The Naito Foundation to M.I.; by Takeda Science Foundation to M.I, and by the Shiseido Female Researcher Science Grant to M.I. This work was partially supported by RIKEN Epigenome Control Program, Medical Research Center Initiative for High Depth Omics, and JST CREST (JPMJCR16G3 and JPMJCR1926) to I.N. **Author contributions:** M.I. conceived and designed the research. N.O., S.K., M.S., Y.D., A.I., A.K., T.S., and M.I. performed experiments. Y.S., T.I., and T.T. analyzed data. I.N., K.S., and M.I. supervised the project. M.I. wrote the manuscript with the input from all the other authors. **Competing interests:** Y.S. and I.N.

consult for Knowledge Palette Inc. and are on their Scientific Advisory Board. The other authors declare that they have no competing interests. **Data and materials availability:** Next-generation sequence data from this article can be found under the following accession numbers: bulk time-course RNA-seq data, DRR429264-DRR429287; scRNA-seq data, GSE227564 (www.ncbi.nlm.nih.gov/geo/query/acc.cgi?acc=GSE227564). All data needed to evaluate the conclusions in the paper are present in the paper and/or the Supplementary Materials.

Submitted 20 January 2023
Accepted 5 June 2023
Published 7 July 2023
10.1126/sciadv.adg6983